Supplement of Atmos. Meas. Tech., 19, 2009–2023, 2026
https://doi.org/10.5194/amt-19-2009-2026-supplement

Atmospheric Measurement Techniques
Open Access
EGU

Supplement of

A novel short-pathlength photoreactor to study aqueous-phase photochemistry: application to biomass-burning phenols

Christopher Niedek et al.

Correspondence to: Qi Zhang (dkwzhang@ucdavis.edu)

Section S1: Determination of the loss rate of GA and 2-NB

The method for calculating the loss rate of GA was adapted from Smith et. al (2014). Because direct measurements of photon flux were not available, the wavelength-resolved photon flux of the SPP light source, I_λ', was estimated using

$$I'_\lambda = \frac{j_{2-NB}}{[2.303 * \Phi_{2-NB} * L * \sum_\lambda (\varepsilon_{2NB} * I_r)} \quad \text{(S1)}$$

where $j_{2\text{-NB}}$ is the photolysis rate constant measured on the day of the experiment (Galbavy et al., 2010), $\Phi_{2\text{-NB}}$ is the quantum yield for 2-NB photolysis, l is the pathlength, $\varepsilon_{2\text{-NB}}$ is the molar absorptivity of 2-NB, and I_r is the relative photon flux of the SPP light source normalized to a maximum of 1.

The rate constant for light absorption by DMB was then calculated as:

$$j_{hv,abs} = 2.303 * \sum_\lambda (\varepsilon_{DMB} * I'_\lambda * L * \Delta\lambda) \quad \text{(S2)}$$

where ε_{DMB} is the molar absorptivity of DMB.

This value was then used to calculate the production rate of triplet-state DMB ($^3DMB^*$):

$$P_{3DMB*} = j_{\text{hv,abs}} * [\text{DMB}]_0 * \Phi_{ISC} \quad \text{(S3)}$$

where $[DMB]_0$ is the initial DMB concentration and Φ_{ISC} is the quantum yield for the intersystem crossing of $^1DMB^*$ to $^3DMB^*$, equal to 0.095 (Ma et al., 2021).

The fraction of $^3DMB^*$ reacting with GA is given by:

$$f_{GA,DMB} = \frac{k_{GA,DMB} * [GA]_0}{(k_{GA,DMB} * [GA]_0 + k_{O2,DMB} * [O_2])} \quad \text{(S4)}$$

where $k'_{GA,DMB}$ is the second-order rate constant for the reaction between GA and $^3DMB^*$ (1.8×10^9 M^{-1} s^{-1}) (Ma et al., 2021), $k'_{O2,DMB}$ is the second-order rate constant for the reaction between dissolved O_2 and $^3DMB^*$ (2.8×10^9 M^{-1} s^{-1}) (Kaur and Anastasio, 2018), and $[O_2]$ is the dissolved oxygen concentration. Dissolved O_2 concentrations in salt solutions were determined using the method described in Narita et. al (1983):

$$\log\left(\frac{S}{S_0}\right) = -\sum_i k_i C_i \quad \text{(S5)}$$

where S is the O_2 solubility with and without (S_0) salts, k is solubility constant for dissolved species "i", and C is the molarity of dissolved species "i". Solubility constants for the relevant ions can be found in Narita et. al (1983). For the ammonium sulfate concentration range used here, the O_2 concentration ranged from 284 μM to 185 μM.

The theoretical loss rate of GA ($L_{GA,t}$) is then determined as:

$$L_{GA,t} = P_{3DMB*} * f_{GA,DMB} \quad \text{(S6)}$$

The experimentally determined loss rate of GA ($L_{GA,M}$) is:

$$L_{GA,m} = k'_{GA} * [GA]_0 \quad \text{(S7)}$$

where k'_{GA} is the pseudo-first order rate constant for GA decay.

The decay of 2-NB ($j_{2\text{-NB}}$) was also modeled to assess the ability of the SPP, particularly at short pathlengths, to produce expected photochemical results. The direct photolysis rate of a compound *c* in an absorbing solution is given by:

$$\frac{dc}{dt_\lambda} = \Phi_\lambda * I_\lambda * F_{s\lambda} * F_{c\lambda} \quad \text{(S8)}$$

where Φ_λ is the quantum efficiency for disappearance at a given wavelength λ, I_λ is the incident light irradiance, $F_{s\lambda}$ is the fraction of photons absorbed by the solution, and $F_{c\lambda}$ is the fraction of absorbed photons that are absorbed by *c*. $F_{s\lambda}$ and $F_{c\lambda}$ are given by:

$$F_{s\lambda} = 1 - 10^{-(\alpha_\lambda + \varepsilon_\lambda * [c]) * l} \quad \text{(S9)}$$

$$F_{c\lambda} = \frac{\varepsilon_\lambda [c]}{\alpha_\lambda + \varepsilon_\lambda [c]} \quad \text{(S10)}$$

where α_λ is the molar absorptivity ε_λ of the absorbing compound multiplied by its concentration and *l* is the pathlength. The direct photolysis rate of 2-NB ($j_{2\text{-NB}}$) is then given by:

$$j_{2-NB} = \frac{2303}{N_A} \sum_\lambda \frac{d_c}{d_{t_\lambda}} * [c] \quad \text{(S11)}$$

Section S2: Supplemental figures and tables

Table S1: Chemical information for the salts used in this study.

Name of chemical	MW (g/mol)	Density (g/mL)	Solubility (g/L)	DRH (%)
LiCl	42.39	2.07	84.25	11
$CaCl_2$	110.98	2.15	745	29
$MgCl_2$	95.211	2.32	529	33
$(NH_4)_2SO_4$	132.14	1.77	770	80
Na_2SO_4	142.04	2.68	497	84

Table S2 Calculated [O_2] for each experiment.

Exp. ID	[GA] (mM)	[SO_4] (mM)	[O_2] (mM)
1	0.1	0.104	283.9
2	0.5	0.104	283.9
3	1	0.104	283.9
4	1.5	0.104	283.9
5	2	0.104	283.9
6	0.1	0.104	283.9
7	0.1	0.104	283.9
8	0.5	0.104	283.9
9	1	0.104	283.9
10	2	0.104	283.9
11	2	10	282.8
12	2	100	272.0
13	2	1000	184.6

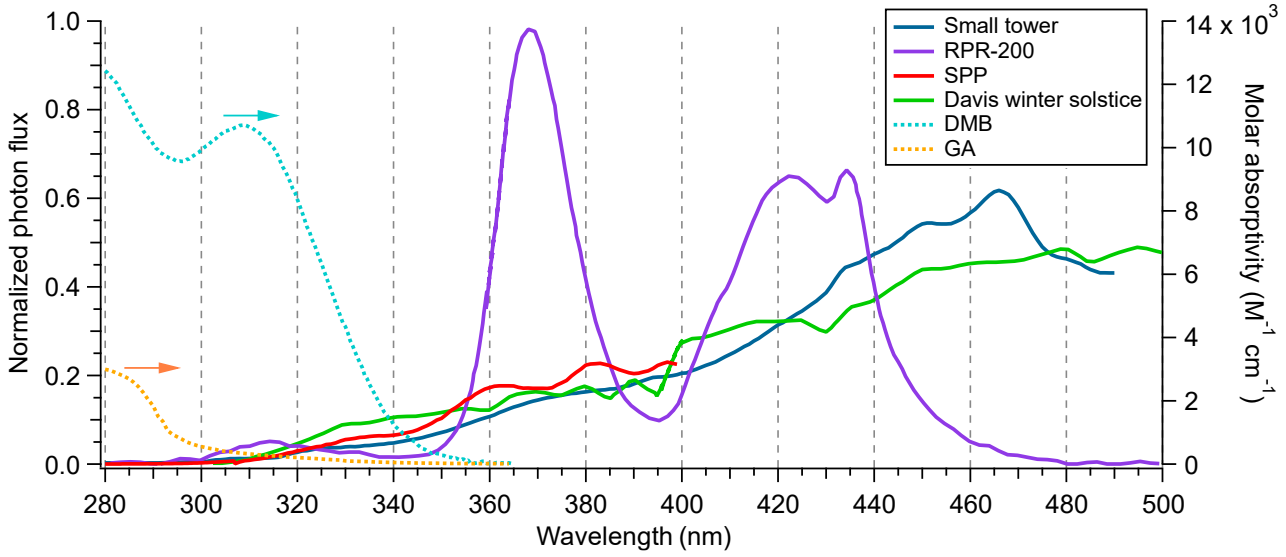

Figure S1: Comparison of the spectral output of the photoreactors evaluated in this study. For reference, the spectrum of tropospheric sunlight during the winter solstice in Davis, CA is included, as both the small tower (ST) and SPP were designed to approximate tropospheric sunlight. The winter solstice photon flux was calculated using the NCAR TUV model (https://www.acom.ucar.edu/Models/TUV/Interactive_TUV/) for Davis, CA on December 21st at a zenith angle of 62°. The absorption spectra of GA and 3,4-DMB are overlaid using the right axis.

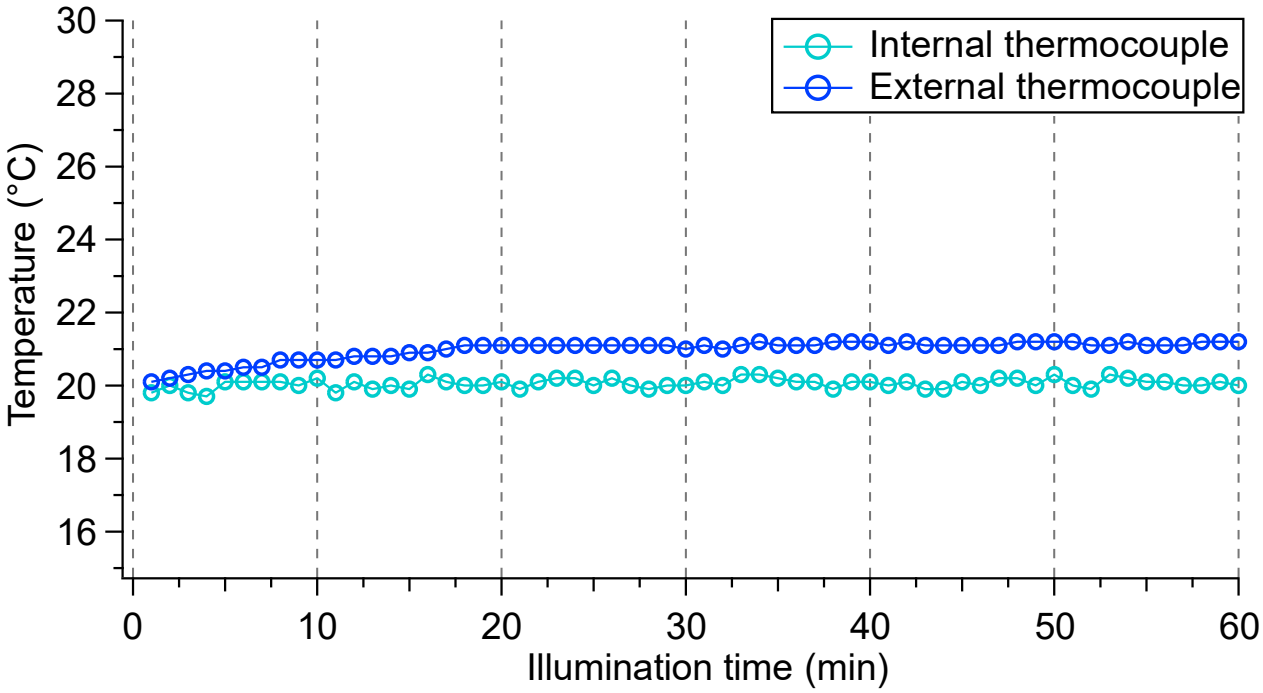

Figure S2: Assessment of temperature stability in the SPP system using the "tall tower" light source and a 1 mM DMB solution. The internal thermocouple is built into the base of the SPP while the external thermocouple was placed directly in the solution.

65

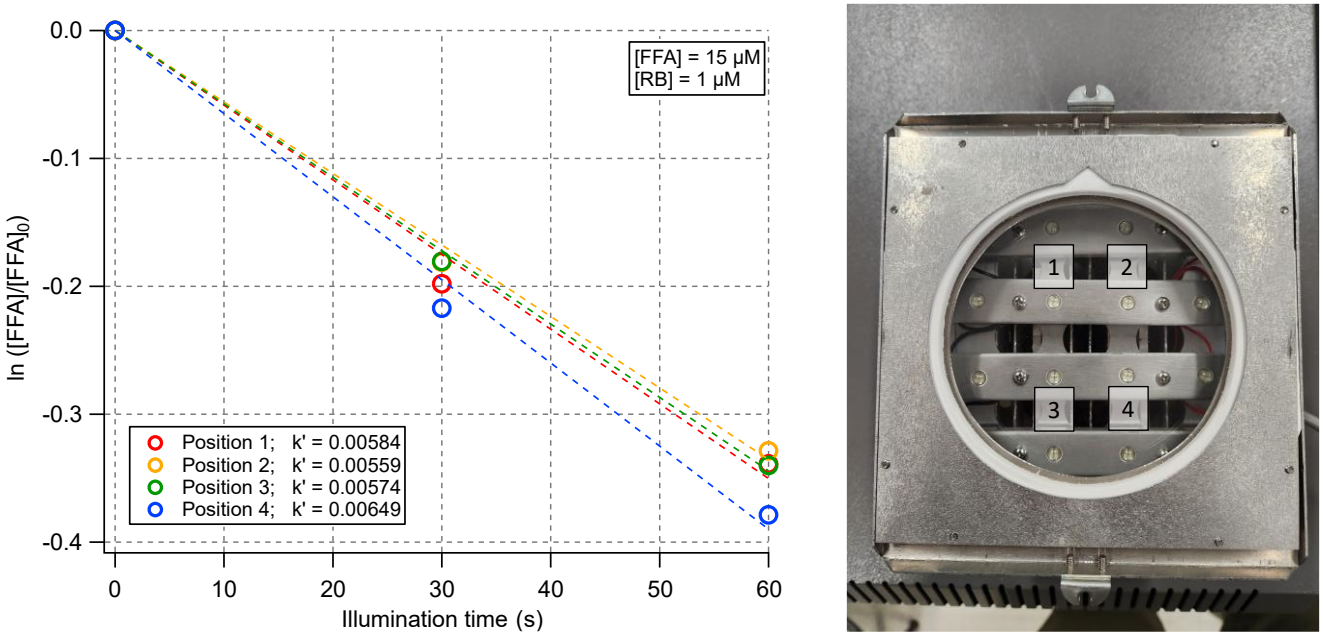

70 **Figure S3: Examination of an alternate, LED array illumination source for the SPP. The left panel shows the measured furfuryl alcohol (FFA) decay rates for photoreactions performed under individual LEDs that make up a larger array. The right panel shows a photograph the LEDs, with the LEDs used in the left panel marked.**

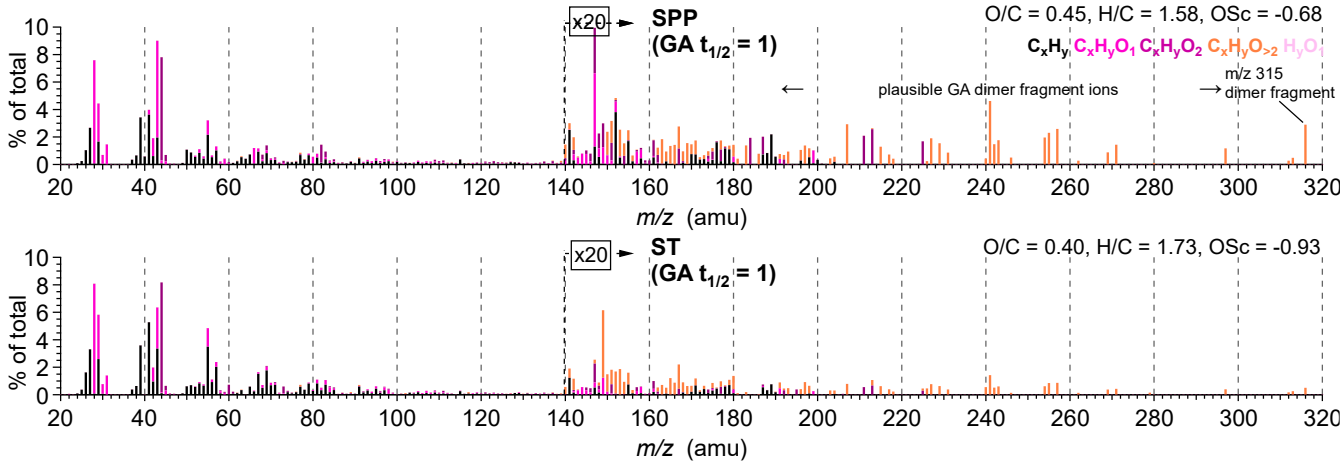

75 **Figure S4: Normalized HRMS for GA+DMB aqSOA produced at the half-life of GA under the same chemical conditions (see experiment 1 in Table 5.5.1 for details) but using the SPP (top) or ST (bottom). Ions with *m/z* ≥ 160 are scaled by a factor of 30 to highlight spectral features at high masses.**

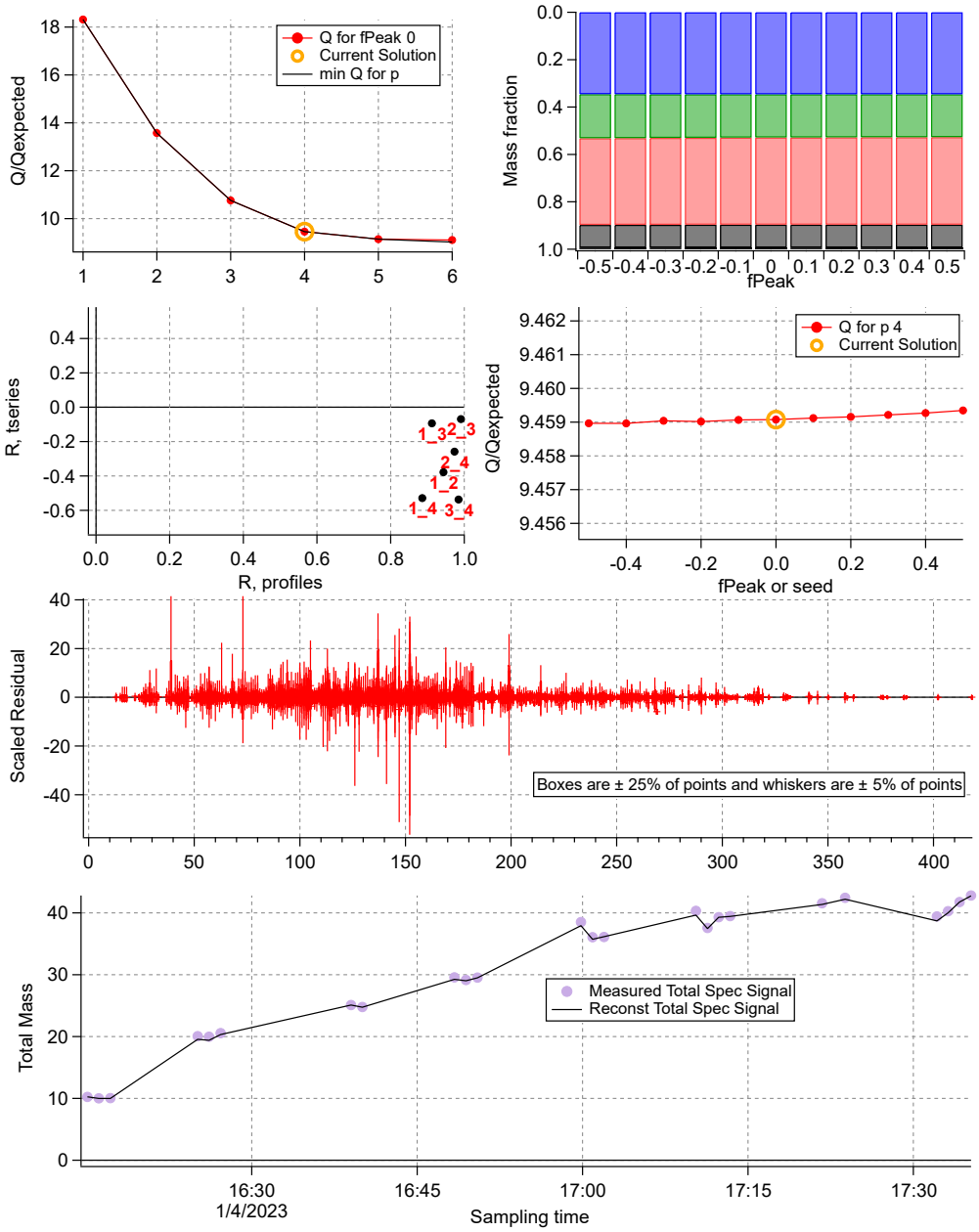

Figure S5: Summary PMF diagnostic plots for Experiment 7.

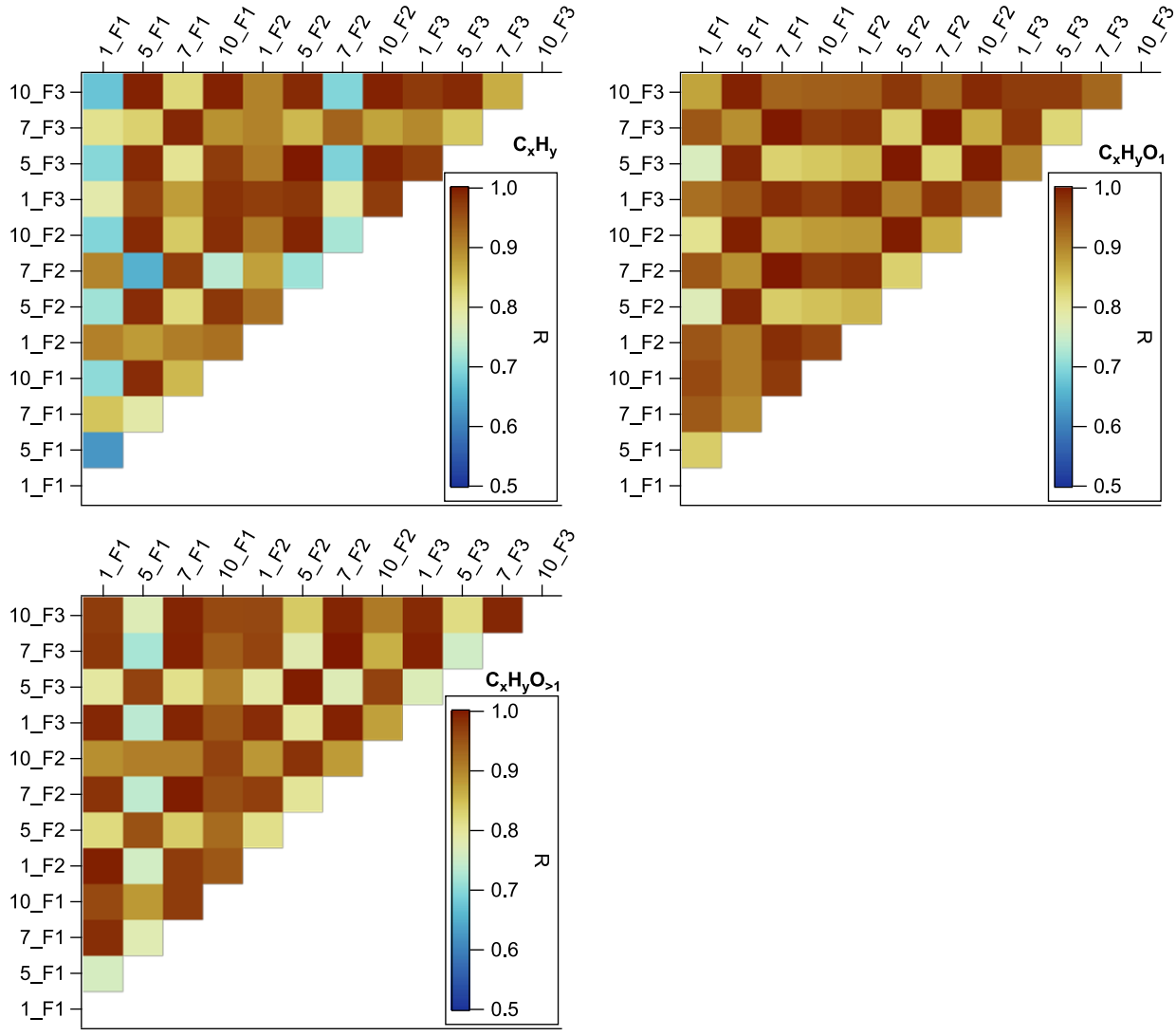

Figure S6: Pearson's r correlations for a subset of the PMF analyses (Exp. ID 1, 5, 7, and 10), selected to represent the extremes of the GA and DMB concentrations examined in this study.

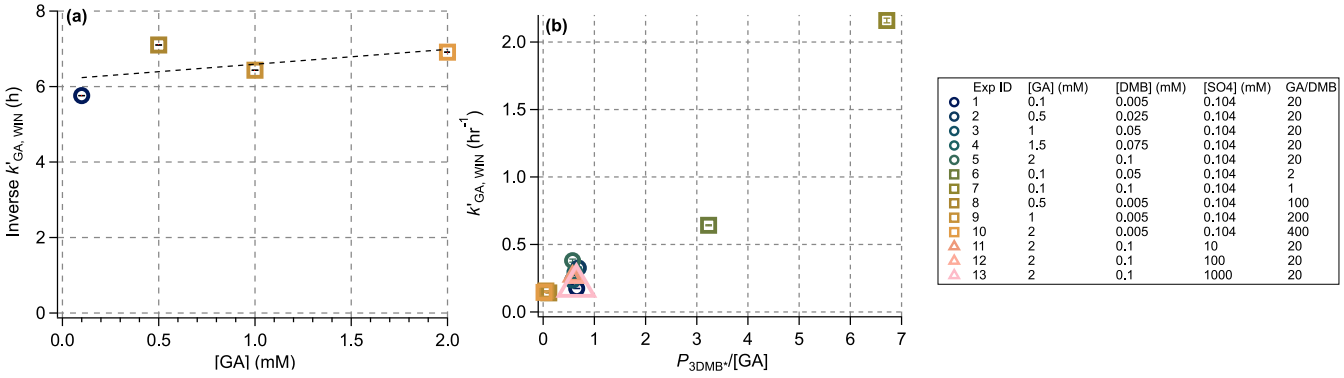

Figure S7: (a) The inverse of $k'_{GA,WIN}$ plotted against [GA], shown only for experiments with the same $[DMB]_0$. Data points connected with the dashed, fit line comprise the series of experiments modifying only [GA] where [DMB] was constant. (b) Measured $k'_{GA,WIN}$ versus calculated P_{3DMB*}/[GA].

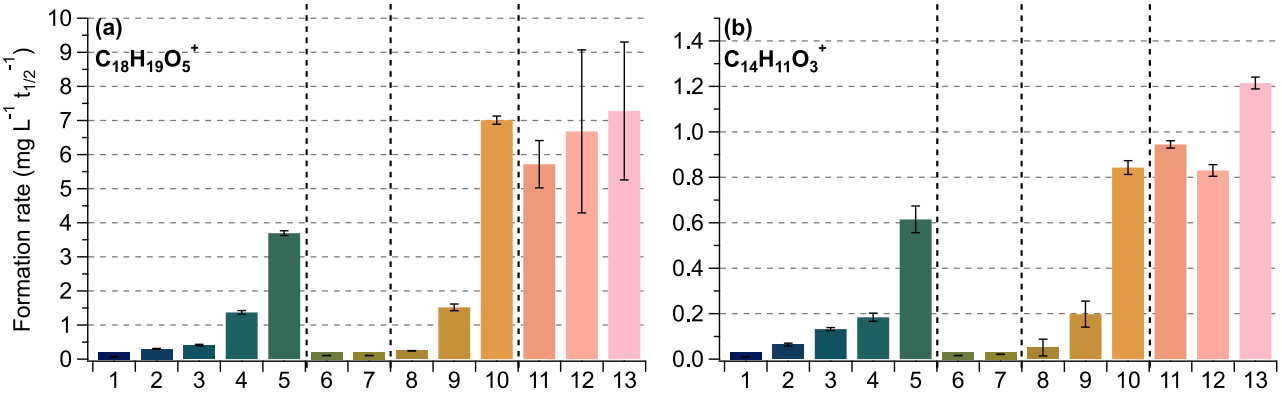

Exp ID	[GA] (mM)	[DMB] (mM)	[SO4] (mM)	GA/DMB
1	0.1	0.005	0.104	20
2	0.5	0.025	0.104	20
3	1	0.05	0.104	20
4	1.5	0.075	0.104	20
5	2	0.1	0.104	20
6	0.1	0.05	0.104	2
7	0.1	0.1	0.104	1
8	0.5	0.005	0.104	100
9	1	0.005	0.104	200
10	2	0.005	0.104	400
11	2	0.1	10	20
12	2	0.1	100	20
13	2	0.1	1000	20

Figure S8: Formation rates of (a) $C_{18}H_{19}O_5^+$ (a major GA dimer tracer ion) and (b) $C_{14}H_{11}O_3^+$ (a likely second-generation product tracer) for individual experiments. Error bars represent propagated uncertainties based on the standard deviations of the fitted coefficients. Reaction conditions are summarized in Table 1 and details regarding the rate-fitting procedures are provided in Section 2.5. All experimental data were fit using single-exponential functions, except for the $C_{14}H_{11}O_3^+$ in Experiments 11-13, where a linear model was used due to poor exponential fit quality. Time-resolved kinetic data used to obtain the fitted values are shown in Figure S9.

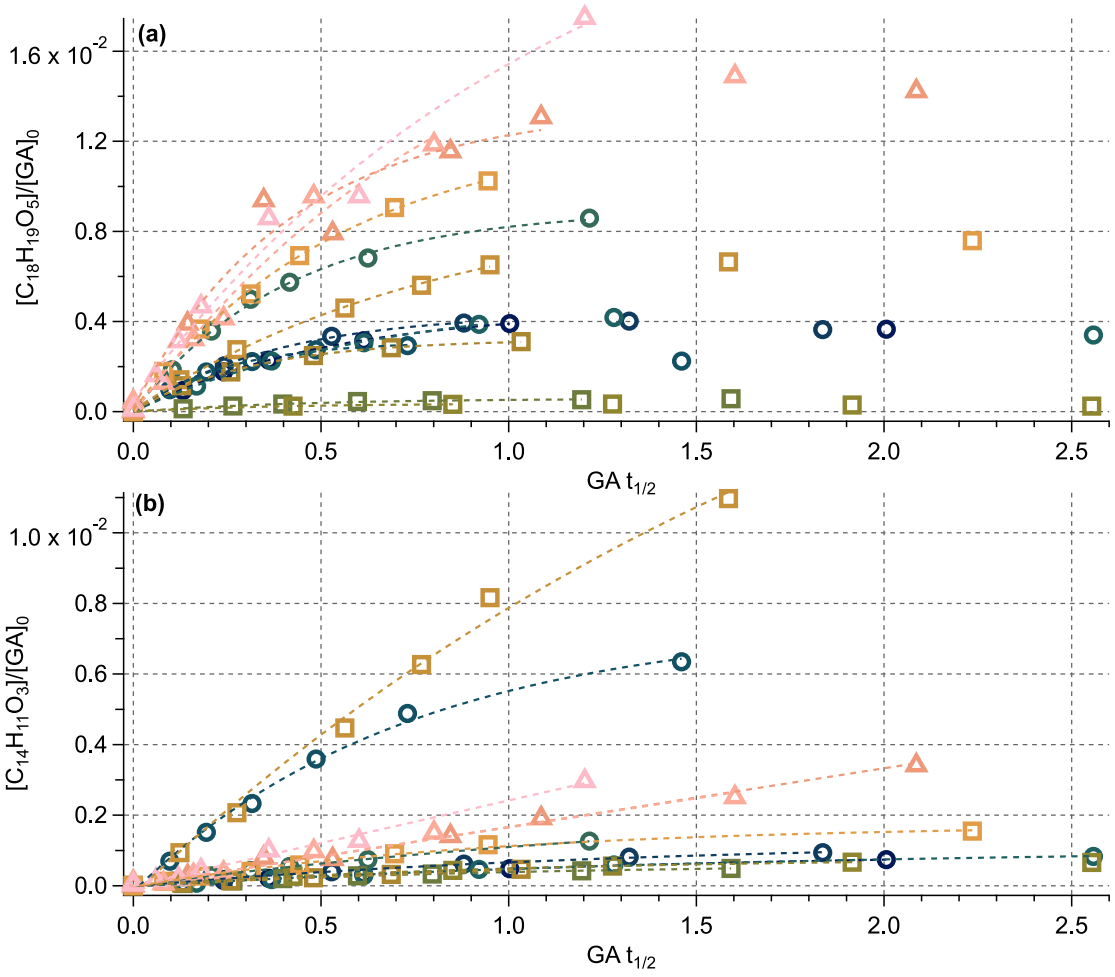

Exp ID	[GA] (mM)	[DMB] (mM)	[SO4] (mM)	GA/DMB
1	0.1	0.005	0.104	20
2	0.5	0.025	0.104	20
3	1	0.05	0.104	20
4	1.5	0.075	0.104	20
5	2	0.1	0.104	20
6	0.1	0.05	0.104	2
7	0.1	0.1	0.104	1
8	0.5	0.005	0.104	100
9	1	0.005	0.104	200
10	2	0.005	0.104	400
11	2	0.1	10	20
12	2	0.1	100	20
13	2	0.1	1000	20

Figure S9: Time-resolved kinetic measurement data for the fitted values presented in Figure 8.